All-Optical Noninvasive Control of Unstable Steady States in a Semiconductor Laser

S. Schikora,[1,*] P. Hövel,[2] H.-J. Wünsche,[1] E. Schöll,[2] and F. Henneberger[1]

[1]*Institut für Physik, Humboldt Universität zu Berlin, Newtonstraße 15, 12489 Berlin, Germany*

[2]*Institut für Theoretische Physik, Technische Universität Berlin, Hardenbergstraße 36, 10623 Berlin, Germany*

(Received 7 June 2006; published 20 November 2006)

All-optical noninvasive control of a multisection semiconductor laser by means of time-delayed feedback from an external Fabry-Perot cavity is realized experimentally. A theoretical analysis, in both a generic model as well as a device-specific simulation, points out the role of the optical phase. Using phase-dependent feedback we demonstrate stabilization of the continuous-wave laser output and noninvasive suppression of intensity pulsations.

DOI: 10.1103/PhysRevLett.97.213902 PACS numbers: 42.60.Mi, 02.30.Ks, 05.45.Gg, 42.55.Px

Unstable states play an important role in complex systems. They frequently interconnect attractors in phase space and thus form the skeleton of the nonlinear dynamics. Instabilities are born in various types of bifurcations. Prominent examples are saddles in saddle-node bifurcations or unstable periodic orbits in the period-doubling route to chaos. Bifurcation analysis, well developed for ordinary and delay-differential equations, can in general uncover also the unstable objects of the phase portrait. The experimental study of unstable states, however, is difficult, because they are visited at most for short times only. Noninvasive control can overcome this difficulty: It stabilizes unstable states but does not change the states themselves, since the control forces act only if the system deviates from the state to be stabilized. Among the various methods, time-delayed feedback control (TDFC) plays an outstanding role [1], as detailed knowledge of the target state is not required here. The control signal is built from the difference $s(t) - s(t-\tau)$ between the present and an earlier value of an appropriate system variable s. TDFC becomes noninvasive for orbits with period τ or steady states [2], because $s(t) = s(t-\tau)$. Involving no numerically expensive computations, it is capable of controlling systems with very fast dynamics still in real-time mode.

TDFC has been applied successfully to the stabilization of periodic orbits in a variety of systems in physics, chemistry, biology, and medicine [3], but much less is known about its action upon steady states. From a practical point of view, it is often desirable to suppress self-sustained oscillations, e.g., in order to stabilize continuous-wave (cw) operation of lasers [4].

In the present Letter, TDFC of unstable steady states in a semiconductor laser device is demonstrated in theory and experiment. Recently, multisection lasers with their complex dynamical phenomena have opened up new ways in high-speed optical information processing [5]. Their picosecond response times are too short even for a fast electronic realization of TDFC. All-optical control as described in this Letter is thus the only applicable method so far. The scheme of the setup is shown in Fig. 1. An integrated tandem laser (ITL) [5] is deliberately driven through a Hopf bifurcation into a self-pulsating regime of operation. Suppression of the pulsations and noninvasive stabilization of the steady state is achieved by direct optical feedback from a properly designed external Fabry-Perot (FP) etalon. Although proposed about a decade ago [6,7] and despite of some numerical studies [7,8], such a noninvasive all-optical control approach has not yet been implemented experimentally. A novel aspect of our analysis is that it addresses the role of the optical phase as a specific feature of the FP control configuration.

Optical fields emitted by lasers vary generally as $\mathrm{Re}\{E(t)e^{-i\omega_0 t}\}$ where the exponential factor oscillates by orders of magnitude faster than the slow amplitude $E(t)$. The field fed back from the FP has the same shape, and for feedback gain K, its amplitude reads as

$$E_b(t) = -Ke^{i\varphi}\sum_{n=0}^{\infty} R^n e^{in\phi}[E(t_n) - e^{i\phi}E(t_{n+1})], \qquad (1)$$

with $t_n = t - \tau_l - n\tau$. The delay originates from a single round-trip between laser and FP, characterized by the latency time τ_l, and n round trips of time τ within the FP of mirror reflectivity R. Two optical phase shifts $\varphi = \omega_0\tau_l$ and $\phi = \omega_0\tau$ are associated with these delay times. Noninvasive control requires optical target states with $E(t) = e^{i\phi}E(t-\tau)$ [9]. For steady states $E(t) = E_0$ this means $e^{i\phi} = 1$; i.e., the FP must be tuned into resonance.

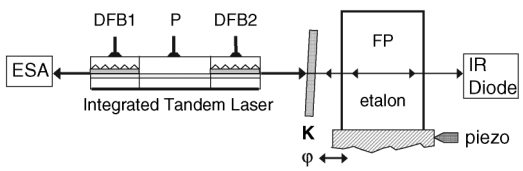

FIG. 1. Scheme of the ITL device with optical feedback from an external FP etalon. Two distributed feedback (DFB) lasers are connected via a passive waveguide section P. Amplitude K and phase φ of the feedback from the FP are controlled by a variable neutral density filter and a piezo positioning, respectively. ESA: electrical spectrum analyzer. IR diode: power measurement.

While the FP phase is thus fixed, the latency is still arbitrary and makes the feedback phase-sensitive. Conventional TDFC corresponds to $\varphi = 0$. However, in the FP geometry, φ is tunable by subwavelength changes of the ITL-FP separation and thus represents an additional free parameter which all-optical TDFC can profit from. In what follows, this is theoretically demonstrated first by a general treatment relying on a two-variable center-manifold model [2] and subsequently in a device-specific numerical simulation resolving fully the spatiotemporal dynamics in the ITL.

We consider a nonlinear system closely above a Hopf bifurcation, where it has an unstable fixed point (focus) whose stability is governed by the complex eigenvalues $\lambda \pm i\omega$ (with $\lambda > 0$). For simplicity, we restrict ourself to a single FP round trip ($n = 0$) and ignore τ_l in the slow amplitude dynamics. Linearizing around the fixed point provides a generic equation for the center-manifold coordinates x, y, corresponding to the complex field through $E = E_0 + x + iy$,

$$\begin{pmatrix} \dot{x} \\ \dot{y} \end{pmatrix} = \begin{pmatrix} \lambda & \omega \\ -\omega & \lambda \end{pmatrix} \begin{pmatrix} x \\ y \end{pmatrix} - K \begin{pmatrix} \cos\varphi & -\sin\varphi \\ \sin\varphi & \cos\varphi \end{pmatrix} \begin{pmatrix} x - x_\tau \\ y - y_\tau \end{pmatrix}, \tag{2}$$

where $x_\tau = x(t - \tau)$, $y_\tau = y(t - \tau)$. This equation generalizes the model of Ref. [2] to phase-sensitive feedback and shows that such feedback creates nondiagonal coupling terms [10]. The characteristic equation for the complex eigenvalues Λ reads as

$$\Lambda + Ke^{\pm i\varphi}(1 - e^{-\Lambda\tau}) = \lambda \pm i\omega. \tag{3}$$

Note that this characteristic equation can be solved analytically using the Lambert function, which is defined as the inverse function of $g(z) = ze^z$ for complex z.

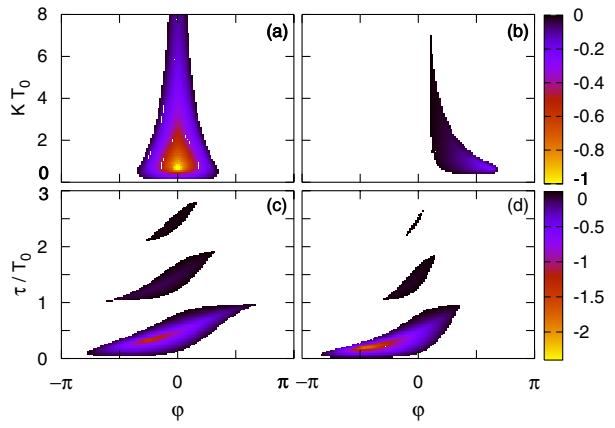

FIG. 2 (color online). Domain of control in dependence on φ, K, and τ with normalization in units of $T_0 = 2\pi/\omega$. The largest real part of the complex eigenvalues Λ is shown in color code. (a),(b) Domain of control in the (φ, K) plane for fixed delay $\tau = T_0/2$ and $0.9T_0$, respectively. (c),(d) Domain of control in the (φ, τ) plane for fixed feedback gain $K = 1/T_0$ and $2/T_0$, respectively. Fixed parameter: $\lambda = 0.2/T_0$.

Figure 2 shows the domain of control, i.e., $\mathrm{Re}(\Lambda) < 0$, dependent on the parameters φ, K, and τ. The unit of time is the intrinsic period $T_0 = 2\pi/\omega$ of the unstable focus and $\lambda T_0 = 0.2$ is chosen in all plots. Panels (a) and (b) represent the (φ, K) plane for fixed values of the time delay $\tau/T_0 = 0.5$ and 0.9, respectively. Note that $\tau = T_0/2$ yields a symmetric domain of control with respect to $\varphi = 0$, which is the case of diagonal coupling [2]. For values other than this optimal time delay, the domain of control is distorted and shrinks. In the situation shown in Fig. 2(b), control can no longer be achieved for $\varphi = 0$, but only for positive phase $\varphi > 0$. Panels (c) and (d) show the domain of control in the (φ, τ) plane for fixed feedback gain $KT_0 = 1$ and 2, respectively. It consists of isolated islands with a horizontal extension that becomes maximum and symmetric with respect to $\varphi = 0$ at delays of $\tau = (n + 1/2)T_0 (n = 0, 1, 2, \ldots)$. No control is possible for integer τ/T_0. For a range of τ values in between, stabilization can be achieved by appropriately chosen φ. When crossing the islands at fixed φ, resonance-type behavior of the damping rate $-\mathrm{Re}(\Lambda)$ occurs. With increasing n, the size of the islands decreases so that they eventually disappear at some critical value determined by the feedback strength K.

The ITL is capable of various Hopf bifurcations; however, the complex spatiotemporal dynamics of the device might induce significant modifications from the generic scenario represented above. We have therefore numerically simulated the ITL-FP configuration on a full device level. Such treatment is also required in order to uncover the specific conditions that have to be met in the experiment. The field-carrier dynamics of the three-section device, combining two distributed feedback (DFB) lasers and a passive waveguide, is treated in the framework of the Maxwell-Bloch equations. By adiabatically eliminating the polarization and including the coupling κ_k between counterpropagating waves in the DFB sections, the slowly varying optical amplitudes $E^{\pm}(z, t)$ and the mean electron-hole pair concentration $n_k(t)$ of each section $k =$ DFB1, P, DFB2 obey the following traveling-wave equations [5]:

$$\left(\frac{1}{c_g}\frac{\partial}{\partial t} \pm \frac{\partial}{\partial z}\right) E^{\pm} = i\beta_k(n_k, S_k)E^{\pm} + i\kappa_k E^{\mp}, \tag{4}$$

$$\frac{dn_k}{dt} = \frac{I_k}{e\sigma L_k} - \frac{n_k}{\tau_n} - \frac{c_g g_k S_k}{1 + \varepsilon_k S_k}. \tag{5}$$

The linear gain $g_k = g_k'(n_k - n_k^{\mathrm{tr}})$, the complex waveguide parameter

$$\beta_k = \delta_k + \alpha_k \frac{g_k}{2} + \frac{i}{2}\left(\gamma_k - \frac{g_k}{1 + \varepsilon_k S_k}\right), \tag{6}$$

and the mean photon density $S_k = \int_k dz(|E^+|^2 + |E^-|^2)$ are quantities that change in time. All other parameters are constants and their values are chosen according to the

device studied experimentally [11]. Continuity of the optical amplitudes at the section interfaces and the antireflection coated end facets is assumed. The feedback (1) from the FP is implemented as a time-delayed boundary condition by setting $E^-(t) = E_b(t)$ and $E(t_n) = E^+(t_n)$, where $E^\pm(t)$ are the amplitudes at the facet opposing the FP.

The bifurcation parameter used in the present context to switch the device output from cw operation to a self-pulsation mode is the internal optical phase shift $\varphi_P = 2L_P\delta_P$ in the passive section. It can be tuned via the static wave number. Figure 3(a) shows the minimum and maximum value of the emitted power taken from transients calculated over a time interval of 8 ns. Equal values mean cw output. The solitary ITL undergoes the relevant Hopf bifurcation at $\varphi_P = 4.277$. Relaxation oscillations (ROs) with a period of $T_0 \approx 89$ ps become undamped here. When a resonant FP with proper feedback parameters is attached, cw operation remains stable beyond this point down to $\varphi_P \approx 3.765$. The feedback signal practically disappears in the whole stabilization range, confirming the noninvasive character of the control.

In Fig. 3(b), the transient dynamics after switching the control on (left part) and off (right part) is depicted. In the first case, the device starts from a free-running stable self-pulsation. After attaching the FP at $t = 0$, the pulsation amplitude starts rapidly to decline. The control signal returned from the FP is initially about 1% of the 15 mW device output, but drops dramatically down to less than 1 pW within 8 ns. After removing the control again, the pulsation recovers. The initial small-amplitude oscillations allow for the determination of the complex eigenvalue $\lambda + i2\pi f$ of the unstable focus. The domain of control obtained by repeating the calculations for a series of different feedback phases φ and feedback strengths K is plotted in Fig. 3(c). It confirms qualitatively the predictions of the generic model for the specific case of the ITL: Stabilization at lowest K appears around $\varphi = 0$, and for larger K, stabilization is only possible in a certain phase range. Note that K is given in different units in Figs. 2(a) and 3(c). At too high K, the stabilization is again lost. This loss is much more abrupt than in the generic model, because additional states of the much more complex phase portrait of the ITL come into play.

The ITL chip used in the experiment has a design as in Ref. [5] except for a larger $L_P \approx 500$ μm. The collimated emission from one of its facets is sent under normal incidence on a quartz-glass etalon [12] and the reflected light is fed back to the ITL along the same path (Fig. 1). The resonance condition $\exp(i\omega_0\tau) = 1$ is adjusted by tuning the lasing mode via device temperature. A variable neutral density filter is used to define the feedback amplitude K. The latency time τ_l is fixed with 5 ps accuracy by positioning the whole FP mounting. Fine-tuning of the FP position

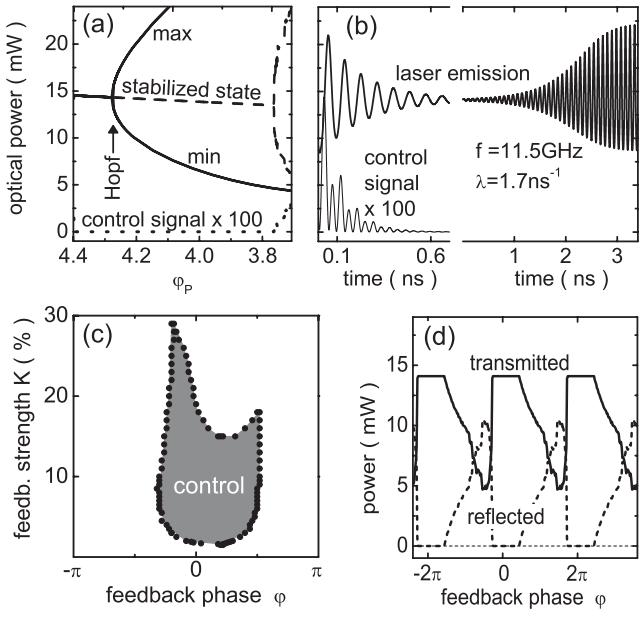

FIG. 3. Control characteristics derived from the device simulation. (a) Maximum and minimum of the laser emission vs internal phase shift φ_P. Solid line, solitary ITL; dashed lines, ITL with lossless FP ($\varphi = 0$, $K = 0.1$, $e^{i\phi} = 1$, $\tau_l = \tau =$ 44.6 ps, mirror reflectivity 70%). Dotted line: time averaged control signal E_b. (b) Output transients after switching control on (left) and off (right); lower left is the control signal. (c) Domain of control in the (φ, K) plane. (d) Transmitted (solid line) and reflected (dashed line) power of the FP for $K = 0.04$. Panels (b)–(d) belong to $\varphi_P = 4.15$.

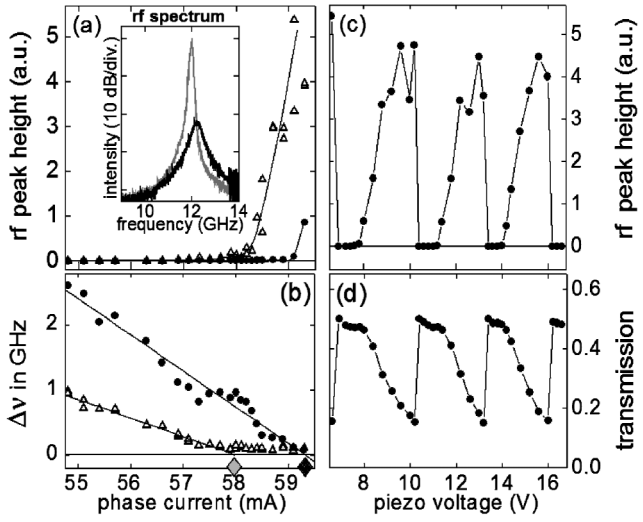

FIG. 4. All-optical TDFC of unstable steady states of an ITL. (a),(b) Height and width ($\Delta\nu$), respectively, of the RO peak in the power spectra versus phase current I_P. Open triangles, solitary ITL; solid circles, with control by the FP. Inset: power spectra at 58.4 mA without (gray) and with (black) control. Diamonds in panel (b): positions of the Hopf bifurcations without (gray) and with (black) FP. (c),(d) Variation of RO peak height and power transmitted through the FP, respectively, versus feedback phase, adjusted here by the piezo voltage. In all measurements, $\tau \approx 38.5$ ps and $\tau_l \approx 120$ ps.

by a piezo actor with subwavelength precision in steps of some 10 nm provides control of the feedback phase φ in a range of several 2π. The mean power transmitted through the FP etalon is detected by an infrared photodiode and provides information on the control signal. The emission from the opposite laser facet is coupled into a fiber, amplified, and analyzed by a 40 GHz electrical spectrum analyzer after optoelectronic conversion by a 50 GHz photodiode.

The Hopf bifurcation considered in the device simulation is experimentally identified from the height and width of the RO peak in the power spectrum. The internal optical phase shift φ_P is changed through the injection current I_P on the passive section. The waveguide has a larger band gap than the DFB sections. Injection modifies its refractive index by free-carrier transitions and, thereby, δ_P. Panels (a) and (b) of Fig. 4 display prototypical data. A sudden increase of the peak height at critical phase current I_P along with a preceding drop of the width is clearly indicative of the bifurcation [13]. Indeed, when adding the properly adjusted FP cavity, the bifurcation point is distinctly shifted to higher phase currents relative to the solitary ITL. As a result of inevitable external and internal noise, there is still a residual RO feature present under control, but its height is suppressed by orders of magnitude [inset of Fig. 4(a)].

Variation of the feedback parameters yields the tendencies expected from the simulations. Control is only possible in a limited range of K. While the generic model assumes $\tau_l = 0$, the minimum latency time of the experimental setup is 120 ps and thus comparable with the period of the ROs. In that case, extra amplitude dynamics is triggered. By increasing τ_l, the parameter range in which control can be achieved shrinks [2,14]. Therefore, in all measurements presented in Fig. 4, the lowest value of τ_l is adjusted. Panel (c) displays the variation of the RO peak height as a function of the ITL-FP separation in the range of several optical periods. Cyclic behavior directly demonstrates the genuine role of the feedback phase φ in all-optical TDFC. The control domain expands over about 30%–40% of a period, in reasonable agreement with the computations. The signal transmitted through the FP is complementary to the control signal fed back into the ITL. The respective data [Fig. 4(d)] follow very closely the theoretical curve in Fig. 3(d). We estimate that the control signal is at least 3 orders of magnitude below the level of the laser emission. Therefore, the control indeed has a noninvasive character.

In conclusion, we have shown that unstable steady states of a semiconductor laser can be noninvasively stabilized by all-optical TDFC. This system is paradigmatic for a large class of nonlinear systems in physics, technology, and beyond. It can be readily manipulated experimentally on small length and fast time scales. Our study demonstrates the crucial importance of the proper choice of phase of the feedback signal, i.e., of the coupling matrix, which represents a generic feature of all-optical TDFC.

This work was supported by Deutsche Forschungsgemeinschaft within Sfb 555. The authors thank Bernd Sartorius (Fraunhofer-HHI Berlin) for providing the ITL, and Mindaugas Radziunas (WIAS Berlin) for his code LDSL-tool.

*Electronic address: schikora@physik.hu-berlin.de

[1] K. Pyragas, Phys. Lett. A **170**, 421 (1992).
[2] P. Hövel and E. Schöll, Phys. Rev. E **72**, 046203 (2005).
[3] H. G. Schuster, *Handbook of Chaos Control* (Wiley-VCH, Weinheim, 1999).
[4] Z. Gills *et al.*, Phys. Rev. Lett. **69**, 3169 (1992); A. Ahlborn and U. Parlitz, Phys. Rev. Lett. **96**, 034102 (2006).
[5] S. Bauer *et al.*, Phys. Rev. E **69**, 016206 (2004); H.-J. Wünsche *et al.*, Phys. Rev. Lett. **94**, 163901 (2005).
[6] J. E. S. Socolar, D. W. Sukow, and D. J. Gauthier, Phys. Rev. E **50**, 3245 (1994).
[7] W. Lu and R. G. Harrison, Opt. Commun. **109**, 457 (1994).
[8] C. Simmendinger and O. Hess, Phys. Lett. A **216**, 97 (1996); V. Z. Tronciu *et al.*, Phys. Rev. E **73**, 046205 (2006).
[9] Feedback from a FP has been studied previously; see, e.g., B. Dahmani, L. Hollberg, and R. Drullinger, Opt. Lett. **12**, 876 (1987); Ph. Laurent *et al.*, IEEE J. Quantum Electron. **25**, 1131 (1989); M. Peil *et al.*, Phys. Rev. A **73**, 023805 (2006); H. Erzgräber *et al.*, Phys. Rev. E **73**, 055201(R) (2006) and references therein. However, those configurations rely on maximum feedback, are thus strongly invasive, and the type of self-organization is principally different from the present one.
[10] M. Rosenblum and A. Pikovsky, Phys. Rev. E **70**, 041904 (2004).
[11] Parameters of device simulations: group velocity $c_g = c/3.8$, complex Bragg coupling $\kappa = [1, 0, 1] \times (250 + 6i)$ cm^{-1}, linewidth enhancement factor $\alpha = [-5, 0, -5]$, internal optical losses $\gamma = [25, 20, 25]$ cm^{-1}, static wave number at transparency $\delta = [27\,978,$ variable, $17\,910]$ m^{-1}, differential gain $g' = [9, 0, 9] \times 10^{-21}$ m^{-1}, gain compression factor $\varepsilon = [5, 0, 5] \times 10^{-24}$ m^3, transparency concentration $n^{\mathrm{tr}} = [1, 0, 1] \times 10^{24}$ m^{-3}, injection currents $I = [8, 0, 80]$ mA, section lengths $L = [220, 440, 220]$ μm, cross section of active zone $\sigma = 4.5 \times 10^{-13}$ m^2, elementary charge e, and nonlinear recombination rates $n/\tau_n = An + Bn^2 + Cn^3$ ($A = 3 \times 10^8$ s^{-1}, $B = 1 \times 10^{-16}$ m^3 s^{-1}, and $C = 1 \times 10^{-40}$ m^6 s^{-1}). Triple values are given according to [DFB1, P, DFB2].
[12] Etalon parameters: thickness 4 mm, refractive index $\bar{n} = 1.43$, absorption coefficient $\alpha = 0.05$ cm^{-1}, mirror reflectivity and absorbance $R = 0.76$ and $A = 0.005$, respectively, and free spectral range 26 GHz, i.e., round-trip time $\tau = 38.5$ ps.
[13] O. Ushakov *et al.*, Phys. Rev. Lett. **92**, 043902 (2004).
[14] P. Hövel and J. E. S. Socolar, Phys. Rev. E **68**, 036206 (2003).